ISSN: 3007-9640 DOI: https://doi.org/10.70114/acmsr.2026.9.1.P127

Research on a Bridge Virtual Load Test Method Based on Measured Influence Surfaces

Limei Yu [1, a], Dong Wang [1, b], Zecheng Chen [1, c], Tonglin Zhang [1, d] and Xin He [2, e *]

[1] Jilin Provincial Transport Research Institute, Changchun Jilin 130102, China;

[2] College of Transportation, Jilin University, Changchun Jilin 130025, China.

[a] 48657530@qq.com, [b] 2524537611@qq.com, [c] 13614328008@163.com,

[d] 1013178297@qq.com, [e] 15116288538@163.com

Abstract. Addressing the limitations of traditional static load testing, which is costly and requires traffic interruption, this paper proposes a virtual load test method based on the measured two-dimensional influence surface of a bridge. Using the two-dimensional strain influence surface identified through moving-vehicle tests, and combined with the principle of linear superposition, the virtual maximum response of a bridge under Highway-Class I standard lane loads is calculated without closing the bridge to traffic. A verification coefficient is obtained by comparison with finite element calculation results, enabling rapid assessment of bridge load-carrying capacity. Taking the old and new bridges of the Songjianghe River Bridge as engineering cases, virtual load tests were conducted on a simply supported hollow slab bridge and a five-span continuous box girder bridge, respectively. The results show that the verification coefficients at all measurement points satisfy the code requirements (0.924–0.995 for the hollow slab bridge and 0.899–0.938 for the continuous box girder bridge); multi-lateral condition analysis based on the influence surface can effectively characterize the force-transfer state of hinge joints in hollow slab bridges, providing a new approach for refined condition assessment of bridges.

Keywords: bridge influence surface; virtual load test; verification coefficient; lateral distribution coefficient; bearing capacity evaluation

1. Introduction

China's highway bridge inventory now exceeds 1.1 million structures, a large proportion of which have entered the mid-to-late stages of their service life, with structural performance degradation becoming an increasingly prominent issue [1]. Periodic load testing is an important technical means of evaluating bridge load-carrying capacity and identifying structural damage [2]. However, conventional static load testing requires prolonged traffic closure and the deployment of numerous heavy loading vehicles, resulting in high implementation costs and severe disruption to operations; achieving full-coverage periodic inspection for the vast number of small- and medium-span bridges is therefore almost infeasible in engineering practice [3]. How to achieve rapid assessment of bridge load-carrying capacity without interrupting traffic has become an important research topic in the field of bridge health monitoring. The current Specification for Highway Bridge Load Testing (JTG/T J21-01-2015) stipulates that the verification coefficient η of a load test must satisfy $\eta \leq 1.0$, and the load efficiency coefficient ηq must satisfy $0.95 \leq \eta q \leq 1.05$, to ensure that the test load can effectively excite the target structural response. However, vehicle loading schemes that satisfy the above requirements are complex to arrange and labor- and time-intensive; how to achieve an equivalent quantitative assessment of load-carrying capacity without on-site vehicle loading therefore remains an engineering challenge that urgently needs to be addressed.

Indirect identification methods offer a new approach to addressing this problem. This class of methods extracts characteristic structural parameters of a bridge from the dynamic coupled response between a moving vehicle and the bridge, without requiring traffic closure [4]. Among these, Yang et al. [5] proposed extracting bridge frequencies from the dynamic response of a passing vehicle, laying the theoretical foundation for indirect identification methods. O'Brien et al. [6] were the first

ISSN: 3007-9640 DOI: https://doi.org/10.70114/acmsr.2026.9.1.P127
to propose a method for identifying influence lines from direct measurement data; Chen et al. [7] subsequently introduced sparse regularization to improve identification stability; Zheng et al. [8] established a dynamic-static separation identification method for high-speed vehicle-passing conditions and systematically reviewed the strengths and weaknesses of existing methods [9]. With the maturation of regularized-inversion theory, the accuracy of influence line identification has continued to improve [10].

Compared with one-dimensional influence lines, two-dimensional influence surfaces simultaneously contain information on both the longitudinal and transverse stiffness distribution of a bridge, enabling a comprehensive characterization of its spatial mechanical behavior, and exhibit higher sensitivity to defects such as hinge-joint damage in hollow slab bridges and abnormal transverse load distribution in multi-girder bridges [11]. Jian et al. [12] proposed an influence surface identification method based on deep learning and computer vision, further extending the technical pathways available for influence surface identification. However, current research on influence surface identification remains largely confined to the methodological level, lacking a systematic approach that directly links identification results to code-specified load-carrying capacity evaluation indices.

To this end, this paper proposes a virtual load test method based on measured two-dimensional influence surfaces: the measured influence surface is used in place of the actual vehicle loading response in conventional static load testing, and, combined with the Highway-Class I standard lane load, the most unfavorable loading condition is automatically determined and the virtual response at each measurement point is calculated, from which the verification coefficient η is obtained; the lateral distribution coefficient is further extracted through multi-lateral condition analysis, enabling rapid assessment of bridge load-carrying capacity without traffic closure. The old and new bridges of the Songjianghe River Bridge are taken as engineering cases for validation, and the technical roadmap of this study is shown in Fig. 1.

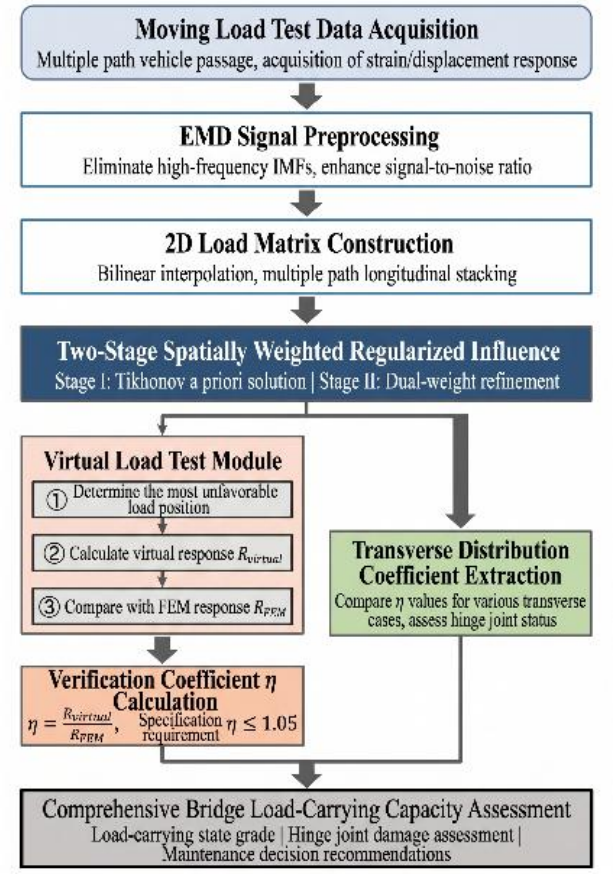


Fig. 1 Technical roadmap of this study

ISSN: 3007-9640 DOI: https://doi.org/10.70114/acmsr.2026.9.1.P127

2. Basic Theory of the Virtual Load Test

2.1 Influence Surface and the Superposition Principle

Let the loading area on the bridge deck be denoted Ω, and let Φ*(x,y) be the two-dimensional strain influence surface identified from the measured data, in units of με/kN. For an arbitrarily distributed load q(x,y), the structural response R at the designated measurement point can be obtained by superposition integration:

$$R = \iint_{\Omega} \Phi^*(x,y) \cdot q(x,y) \cdot dxdy \tag{1}$$

Discretizing the above expression in grid-summation form:

$$R_{virtual} = \Sigma_i \Sigma_j \, \Phi^*(x_i, y_j) \cdot q(x_i, y_j) \cdot \Delta x \Delta y \tag{2}$$

where x_i, y_j are the longitudinal and lateral coordinates of the grid nodes; Δx, Δy are the longitudinal and lateral grid step sizes; and $q(x_i, y_j)$ is the intensity of the standard load at node (x_i, y_j). The influence surface $\Phi^*(x,y)$ is back-calculated from measured data and therefore inherently incorporates the true boundary conditions and stiffness distribution of the structure, so the virtual response $R_{virtual}$ can reflect the true mechanical state of the structure.

2.2 Brief Description of the Identification Method

This paper adopts the two-stage spatially weighted regularization method disclosed in an authorized invention patent [14] (patent No. ZL 2026 1 0194457.3), extended to two-dimensional influence surface identification. In the first stage, standard Tikhonov regularization is used to solve for a preliminary influence surface Φ_0, with the optimization objective function:

$$\min_{\Phi} \|L\Phi - R\|_2^2 + \lambda^2 \|T_{2D}\Phi\|_2^2 \tag{3}$$

where L is the load matrix; R is the measured response vector; λ is the regularization parameter, determined automatically by the L-curve criterion; and T_{2D} is the two-dimensional discrete Laplacian coupling operator constructed from the Kronecker product:

$$T_{2D} = (I_{ny} \otimes D_x) + (D_y \otimes I_{nx}) \tag{4}$$

where D_x, D_y are the one-dimensional second-order difference matrices in the longitudinal and lateral directions, respectively, and $\otimes$ denotes the Kronecker product operator; this simultaneously constrains the longitudinal and lateral smoothness of the influence surface.

In the second stage, based on the peak locations in Φ_0, a spatially adaptive smoothing weight matrix W_l and a background-structure-preserving weight matrix W_s are constructed, establishing the dual-weight co-optimization objective function:

$$\min_{\Phi} \|L\Phi - R\|_2^2 + \lambda^2 \|W_l T_{2D}\Phi\|_2^2 + \lambda^2 \|W_s(\Phi - \Phi_0)\|_2^2 \tag{5}$$

The three terms are the data-fidelity term, the spatially adaptive smoothing term, and the background-structure-preserving term, respectively. W_l approaches zero in the peak region to release the smoothing constraint and achieve high-fidelity recovery of the peak; W_s anchors the solution to the prior baseline Φ_0 outside the peak protection region, preventing drift in the background region. Eq. (5) is equivalently transformed into an augmented least-squares form:

$$A = [L;\ \lambda W_l T_{2D};\ \lambda W_s],\ b = [R;\ 0;\ \lambda W_s \Phi_0] \tag{6}$$

The LSQR iterative algorithm is used to solve $\min\|A\Phi - b\|_2$, with the augmented matrix A stored in CSR sparse format, effectively resolving the memory-consumption bottleneck of the two-dimensional, high-dimensional sparse system of equations. The mean deviation between the identification results and the core measurement points of the Abaqus finite element simulation is 2.67%.

ISSN: 3007-9640 DOI: https://doi.org/10.70114/acmsr.2026.9.1.P127

2.3 Determination of the Most Unfavorable Load Position

(1) Position of the concentrated load Pk: the coordinates of the point of maximum absolute value on the influence surface, (xpeak, ypeak), are taken, i.e.:

$$(x_{peak}, y_{peak}) = argmax_{(x,y)\in\Omega} |\Phi^*(x,y)| \tag{7}$$

(2) Loading interval of the uniformly distributed load q_k: loading is applied longitudinally over the entire positive-value region ($\Phi^* > 0$), and laterally over the standard lane width; the lateral position is taken as the lane centerline position that produces the maximum response.

(3) For continuous girder bridges, the most unfavorable loading scheme is determined separately for the mid-span sections (positive-moment controlling sections) and the intermediate-support sections (negative-moment controlling sections): for the mid-span section, uniformly distributed loads are applied in the span under consideration and all spans with influence-surface values of the same sign; for the support section, uniformly distributed loads are applied to the negative-value regions of the two spans adjacent to the support, with the concentrated load applied at the support. The most unfavorable load positions are illustrated in Fig. 2.

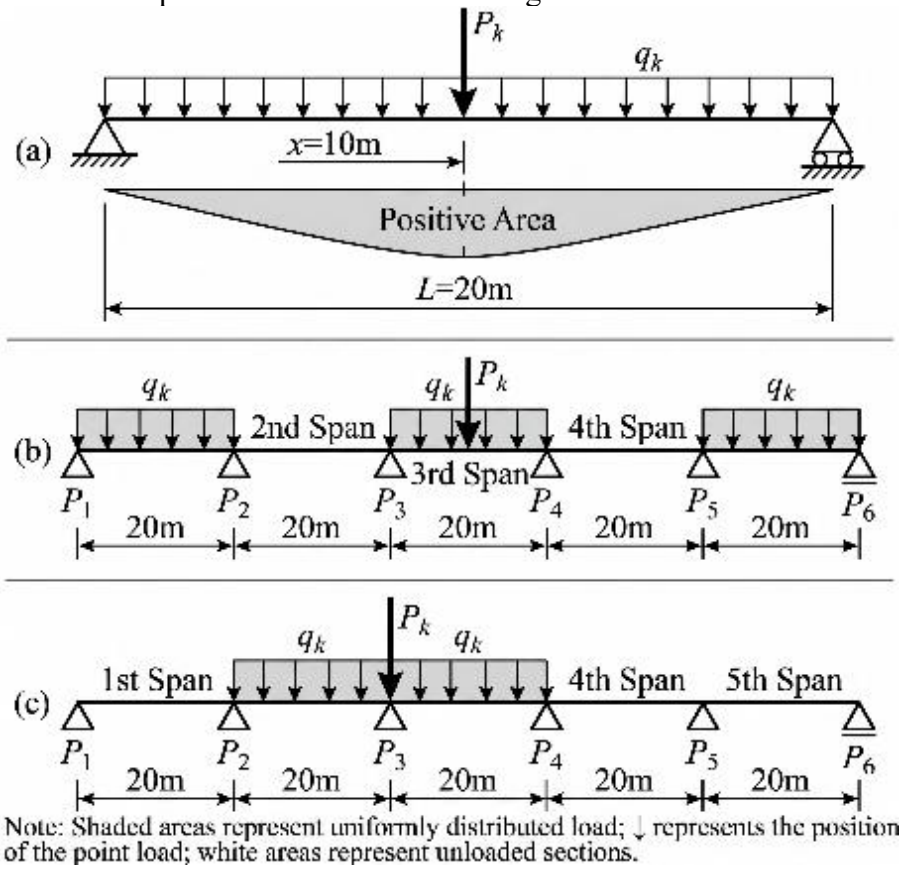


Fig. 2 Schematic diagram of the most unfavorable load positions

2.4 Verification Coefficient and Load Efficiency Coefficient

Referring to the definition of the load-test verification coefficient in JTG/T J21-01-2015 *Specification for Highway Bridge Load Testing* [2], the verification coefficient η of the influence-surface-based virtual load test is defined as:

$$\eta = R_{virtual} / R_{FEM} \tag{8}$$

where $R_{virtual}$ is the virtual maximum response calculated from the measured influence surface, and R_{FEM} is the theoretical maximum response of the finite element model under the same standard loading condition. The code requires $\eta \leq 1.0$.

ISSN: 3007-9640 DOI: https://doi.org/10.70114/acmsr.2026.9.1.P127

The load efficiency coefficient η_q is defined as the ratio of the actual loading effect to the design loading effect, with the code requiring $\eta_q \geq 0.95$. When loading with a single vehicle does not satisfy this requirement, the number of vehicles is increased until it is satisfied:

$$\eta_q = \Sigma\varepsilon_{e,k} / S_{design} \geq 0.95 \tag{9}$$

where $\Sigma\varepsilon_{e,k}$ is the superposition of strains produced by all loading vehicles, and S_{design} is the design load effect calculated according to the code (the full-span integral value of the Highway-Class I lane load).

3. Engineering Case and Test

3.1 Project Overview

The Songjianghe River Bridge is located on National Highway G331 in Jilin Province and consists of an old and a new carriageway. The old carriageway is a reinforced simply supported hollow slab bridge with a single span of 20 m, comprising 10 hollow slabs, a clear deck width of 9.5 m (two lanes), and a Highway-Class I design load level; the new carriageway is a newly built five-span continuous box girder bridge (5×20 m) with a clear deck width of 8.5 m (two lanes) and a Highway-Class I design load level. The two carriageways together form the Songjianghe River double-carriageway bridge, the general layout of which is shown in Fig. 3.

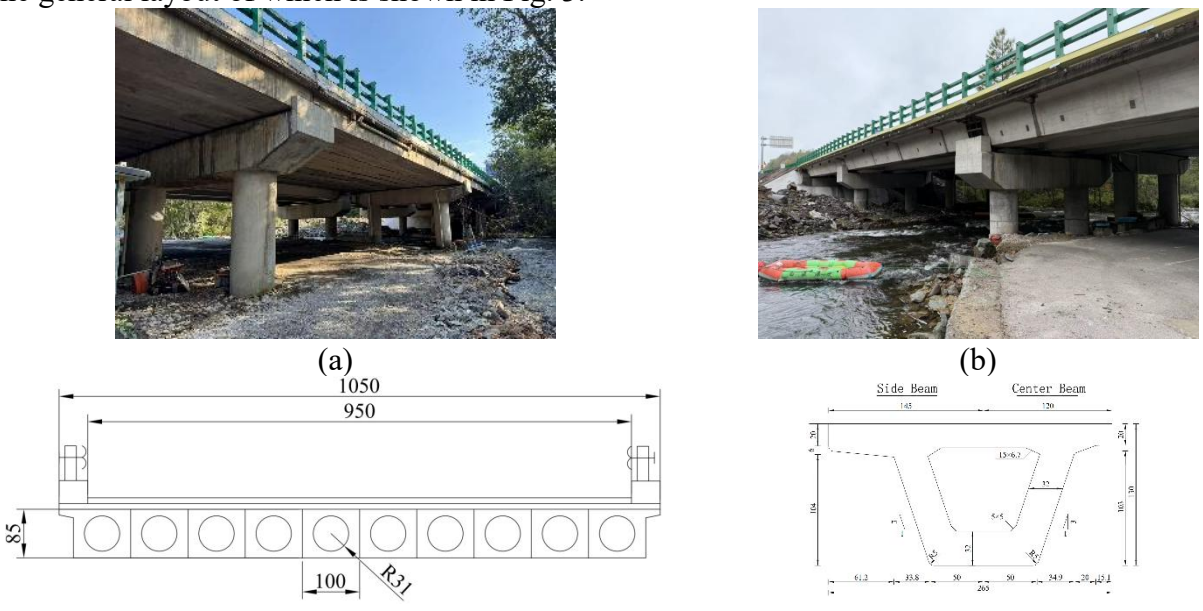


Fig. 3 Overview of the bridge under investigation: (a) panoramic photo of the old carriageway; (b) panoramic photo of the new carriageway; (c) cross-sectional schematic (units: mm)

3.2 Test Scheme and Sensor Layout

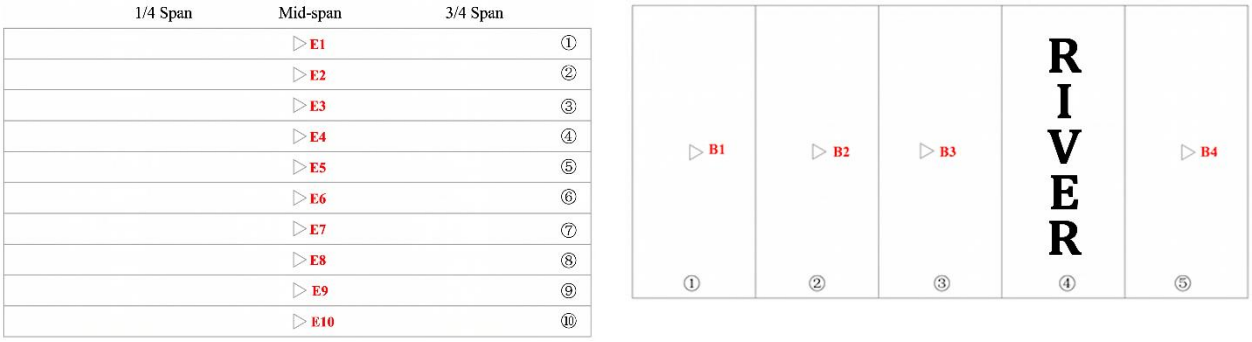
The test vehicle was a four-axle fully loaded truck with axle weights P1 = 2.94 t, P2 = 10.66 t, P3 = 19.16 t, and P4 = 13.56 t, axle spacings D1 = 1.95 m, D2 = 2.28 m, and D3 = 1.32 m, and a total weight of 46.32 t. The vehicle traveled at a constant speed of 20 km/h along multiple parallel lateral paths across the deck, with a lateral spacing between paths of approximately half the vehicle width (about 1.0 m), covering the full width of the bridge.

On the simply supported hollow slab bridge, strain gauges were affixed to the soffit of each slab at the mid-span section, giving a total of 10 measurement points (E1–E10, labeled sequentially from left to right); this paper selects the representative points E1, E3, E5, E7, and E9 for analysis. On the continuous box girder bridge, four measurement points (B1–B4) were arranged at the mid-span of each span; the sensor layout is shown in Fig. 4. Strain signals at each point were synchronously acquired at a sampling frequency of 100 Hz. To improve the quality of the response signals, the raw

ISSN: 3007-9640 DOI: https://doi.org/10.70114/acmsr.2026.9.1.P127

strain time-histories were denoised using Empirical Mode Decomposition (EMD): the raw signal is adaptively decomposed into a sum of several Intrinsic Mode Functions (IMFs), the first k IMF components containing high-frequency vibration noise are identified and removed (k is typically 1–3), and the remaining components are used to reconstruct the low-frequency quasi-static response. EMD denoising requires no pre-set cutoff frequency and can adaptively accommodate the non-stationary, nonlinear characteristics of the vehicle–bridge coupled response; compared with conventional low-pass filtering, it offers stronger signal-fidelity capability, providing an effective data foundation for improving the accuracy of influence surface identification.

During the test, each lateral path was traversed at least 3 times, and the mean of the response time-histories was taken to reduce the influence of random error. The lateral coordinates of the paths were precisely calibrated using pavement markings, with the lateral positioning error controlled within ±0.05 m. The regularization parameter λ used in influence surface identification was determined automatically via the L-curve criterion, without manual intervention.

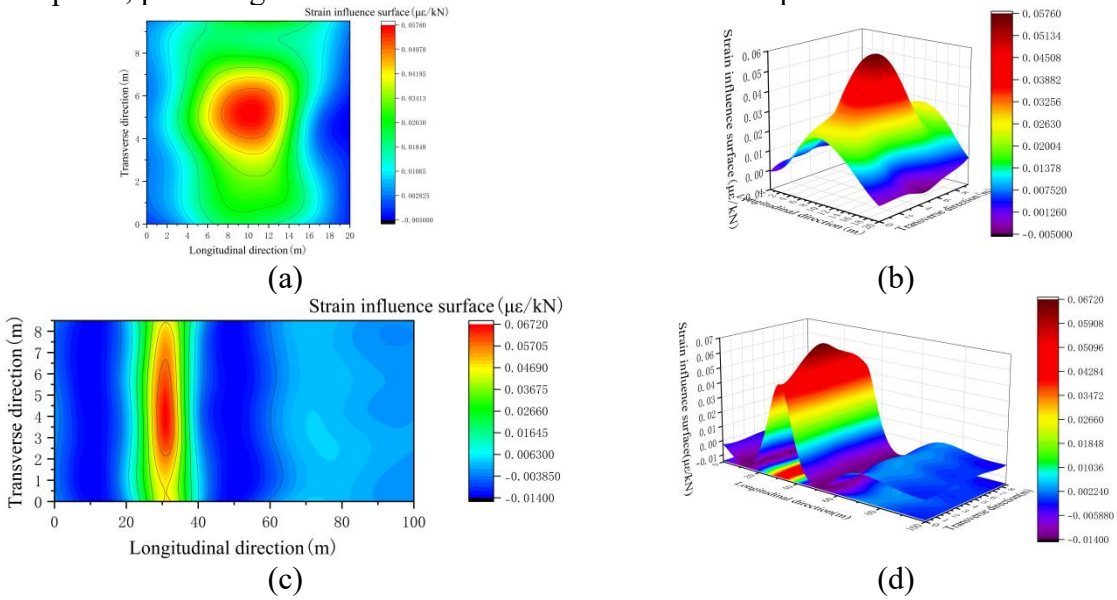


(a) (b)

Fig. 4 Sensor layout: (a) simply supported hollow slab bridge; (b) continuous box girder bridge

3.3 Influence Surface Identification Results

Based on the multi-path test data, the two-dimensional strain influence surface at each measurement point was identified using the method described in Section 2.2. Fig. 5 shows the identified influence surface contour plots and 3D surface plots for the mid-span slab of the hollow slab bridge (E5) and the mid-span of the second span of the continuous box girder bridge (B2). As can be seen from the figure, the resulting influence surfaces are smooth and continuous with clearly defined peaks, providing a reliable data foundation for the subsequent virtual load test calculations.



(a) (b)

(c) (d)

Fig. 5 Identified influence surfaces at representative measurement points (contour and 3D comparison): (a) E5 contour plot; (b) E5 3D surface plot; (c) B2 contour plot; (d) B2 3D surface plot

ISSN: 3007-9640 DOI: https://doi.org/10.70114/acmsr.2026.9.1.P127

4. Virtual Load Test Calculation

The Songjianghe River Bridge is a structure on National Highway G331, with a Highway-Class I design load level. According to JTG D60—2015 [13], the Highway-Class I lane load consists of a superposition of a uniformly distributed load and a concentrated load. The calculated span of both bridges is L = 20 m (single span of 20 m for the simply supported hollow slab bridge; each span of 20 m for the five-span continuous box girder bridge). The load parameters are: standard value of the uniformly distributed load qk = 10.5 kN/m; standard value of the concentrated load Pk = 2(L+130) = 300 kN; standard lane width 3.75 m; with a transverse reduction factor of 1.0 applied for two-lane loading. In this section, the above loads are applied at the most unfavorable position for each measurement point, the virtual loading response at each point is calculated according to Eq. (2), and the verification coefficient is obtained by comparison with the Abaqus finite element results.

4.1 Virtual Loading Results for the Simply Supported Hollow Slab Bridge

The Highway-Class I lane load described above was applied at the most unfavorable position for each measurement point; the results are shown in Table 1, and the distribution of η values is shown in Fig. 6.

Table 1 Virtual load test results at each measurement point of the simply supported hollow slab bridge

Point	Virtual Loading Response (με)	FE Response (με)	Verification Coefficient η
E1	55.4815	58.7723	0.9440
E3	35.5311	36.7421	0.9670
E5	32.8445	35.5641	0.9235
E7	39.3664	39.5804	0.9946
E9	47.8850	50.2222	0.9535

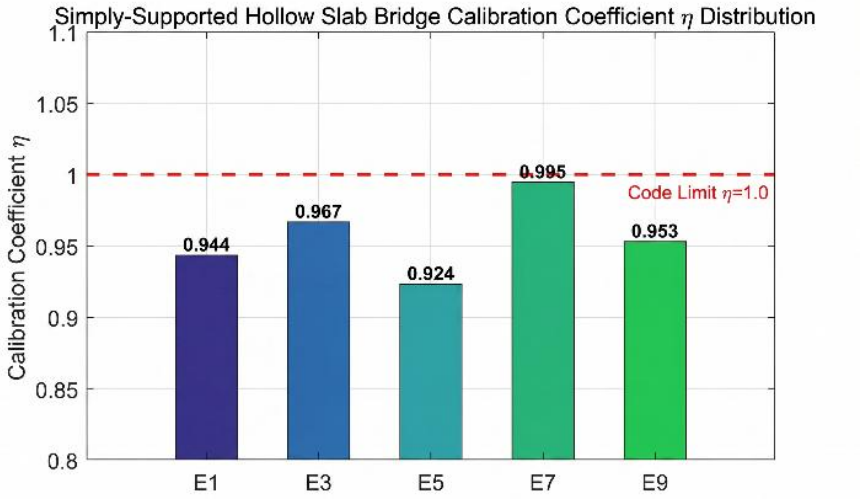


Fig. 6 Distribution of verification coefficients η at each measurement point of the simply supported hollow slab bridge

As shown in Table 1 and Fig. 6, the verification coefficients η at points E1, E3, E5, E7, and E9 range from 0.924 to 0.995, all satisfying the code requirement of $\eta \leq 1.0$, indicating that the load-carrying capacity of the strengthened simply supported hollow slab bridge meets the Highway-Class I design standard. Point E7 has the highest η value (0.995), closest to the code limit, corresponding to the hollow slab nearest to lane 2, which carries the greatest load under two-lane loading and whose actual stiffness most closely matches the theoretical model; point E5 has the lowest η value (0.924), indicating relatively greater stiffness reserve and a larger margin of load-carrying capacity in the mid-

ISSN: 3007-9640 DOI: https://doi.org/10.70114/acmsr.2026.9.1.P127
span slab; the edge slabs E1 (0.944) and E9 (0.953) have intermediate η values, consistent with the typical pattern of lighter loading and greater stiffness reserve in the edge slabs of hollow slab bridges — overall, the strengthening effect is good. In terms of the lateral distribution of η values, E7 (0.995) > E3 (0.967) > E9 (0.953) > E1 (0.944) > E5 (0.924), which is closely related to the distance of each slab position from the lane centerlines under two-lane loading: slab E7 is closest to lane 2 and experiences the greatest load effect under the fully loaded two-lane condition, giving it the highest ratio of virtual response to finite element theoretical value; slab E5 lies between the two lanes and receives some load transfer from both sides, but the contribution from either single lane is less than that at E7, hence its lowest η value. The above distribution pattern is highly consistent with the lateral load-transfer theory of hollow slab bridges, further verifying the accuracy of the influence-surface-based virtual loading method in assessing spatial load effects.

In addition, the η values at all measurement points fall within the range of 0.92–1.00, with a concentrated distribution and low dispersion, indicating that the stiffness distribution across the strengthened slabs is relatively uniform, with no individual slab exhibiting a significantly degraded stiffness that would produce an abnormally high η value — confirming the reliability of the strengthening scheme.

4.2 Virtual Loading Results for the Five-Span Continuous Box Girder Bridge

The same calculation was performed for each measurement point of the five-span continuous box girder bridge; the results are shown in Table 2, and the distribution of η values is shown in Fig. 7.

Table 2 Virtual load test results at each measurement point of the five-span continuous box girder bridge

Point	No. of Vehicles	ηq	Virtual Loading Response (με)	FE Response (με)	Verification Coefficient η
B2	2	0.890	43.8119	48.7327	0.8990
B3	3	0.962	54.5409	58.1562	0.9378

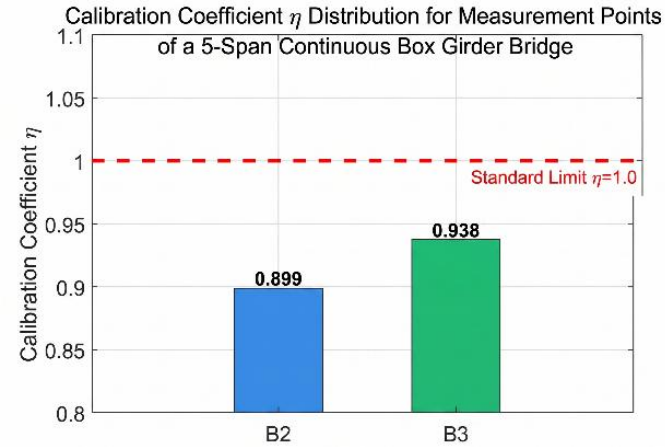


Fig. 7 Distribution of verification coefficients η at each measurement point of the five-span continuous box girder bridge

As shown in Table 2 and Fig. 7, the verification coefficients at points B2 and B3 are 0.899 and 0.938, respectively, both satisfying the code requirement of η ≤ 1.0; the load-carrying capacity rating of the five-span continuous box girder bridge is therefore qualified. For point B2, with multiple vehicles arranged in sequence, the positive-value influence region covers only spans 2 and 4; after loading with 2 vehicles, the load efficiency coefficient ηq = 0.890, which has already reached the practical loading limit of the positive-value region — an inherent characteristic of the limited extent of the positive-value influence region in continuous girders. For point B3, the positive-value region covers spans 1, 3, and 5; after loading with 3 vehicles, ηq = 0.962, satisfying the code requirement.

ISSN: 3007-9640 DOI: https://doi.org/10.70114/acmsr.2026.9.1.P127
The η value at B3 (0.938) is higher than that at B2 (0.899) because B3 is located in span 3, in the middle of the five-span continuous girder, where the positive-value influence region covers three spans (1, 3, and 5), giving a more complete load efficiency and a virtual response closer to the finite element theoretical value. The η values at both points are clearly below 1.0, indicating that the actual stiffness of the newly built continuous box girder bridge exceeds that predicted by the finite element model, with a good reserve of load-carrying capacity. It should be noted that the load efficiency coefficient at point B2 (ηq = 0.890) is slightly below the code requirement of 0.95; this does not reflect inadequate bridge load-carrying capacity, but rather is an inherent mechanical characteristic resulting from the limited extent of the positive-value influence region in continuous girders. In actual static load testing, engineers typically increase ηq artificially by applying reverse loading (inducing negative moment) in the negative-value influence region; however, the virtual loading method in this paper considers only the positive-value loading region and does not apply negative reverse loads, hence the lower ηq. For the condition aimed at evaluating positive-moment bearing capacity, point B2 has η = 0.899 < 1.0, and the structural load-carrying capacity satisfies the requirement — a conclusion unaffected by the slightly low ηq. Future research could further explore incorporating reverse loading of the negative-value influence region into the virtual loading system, to more comprehensively approach the code's load efficiency requirements.

5. Lateral Distribution Coefficient Analysis

The two-dimensional influence surface not only contains information on the longitudinal stiffness of the bridge, but also fully preserves the lateral load-transfer characteristics, providing a direct, quantitative means of assessing the working condition of hinge joints in hollow slab bridges. Hinge joints are the core components providing lateral connectivity in precast hollow slab bridges; cracking damage to a hinge joint causes loss of shear-transfer capability between adjacent slabs, degrading the bridge from coordinated multi-slab action to single-slab action. Existing research has shown [15] that, after hinge-joint damage, the measured strain of the directly loaded slab can be 20%–50% higher than under normal conditions, while the strain of adjacent slabs is correspondingly lower, appearing in lateral-condition comparison plots as a sudden change in curve slope and anomalous crossing of curves. Therefore, systematic comparison of the eccentric-loading verification coefficients of each slab under multiple lateral loading conditions can provide a quantitative assessment of hinge-joint health without requiring an additional dedicated inspection test.

The lane centerline positions for the three lateral loading conditions were set as follows: for the left-eccentric condition, the two lane centerlines were shifted 1.5 m to the left (lane 1 centerline at 1.1 m, lane 2 centerline at 5.3 m); for the central loading condition, the original lane positions were retained (lane 1 centerline at 2.6 m, lane 2 centerline at 6.8 m); for the right-eccentric condition, the two lane centerlines were shifted 1.5 m to the right (lane 1 centerline at 4.1 m, lane 2 centerline at 8.3 m). An offset of 1.5 m, approximately 40% of the standard lane width of 3.75 m, effectively excites the lateral differential response of each slab without exceeding the drivable range of the deck.

This paper defines the eccentric-loading verification coefficient at lateral position y as $\eta(y)$:

$$\eta(y) = R_{virtual}(y) / R_{FEM}(y) \tag{10}$$

Table 3 gives the verification coefficients at each measurement point of the simply supported hollow slab bridge under the three lateral loading conditions — left-eccentric (lane centerlines shifted 1.5 m to the left), central, and right-eccentric (lane centerlines shifted 1.5 m to the right) — and Fig. 8 shows the curves of η at each slab versus the lateral loading position.

Table 3 Verification coefficients at each measurement point of the simply supported hollow slab bridge under eccentric loading conditions

ISSN: 3007-9640 DOI: https://doi.org/10.70114/acmsr.2026.9.1.P127

Point	η (Left-eccentric)	η (Central)	η (Right-eccentric)
E1	1.073	0.954	0.434
E3	0.510	0.967	0.760
E5	0.999	0.924	0.849
E7	0.553	0.995	0.721
E9	0.721	0.944	1.095

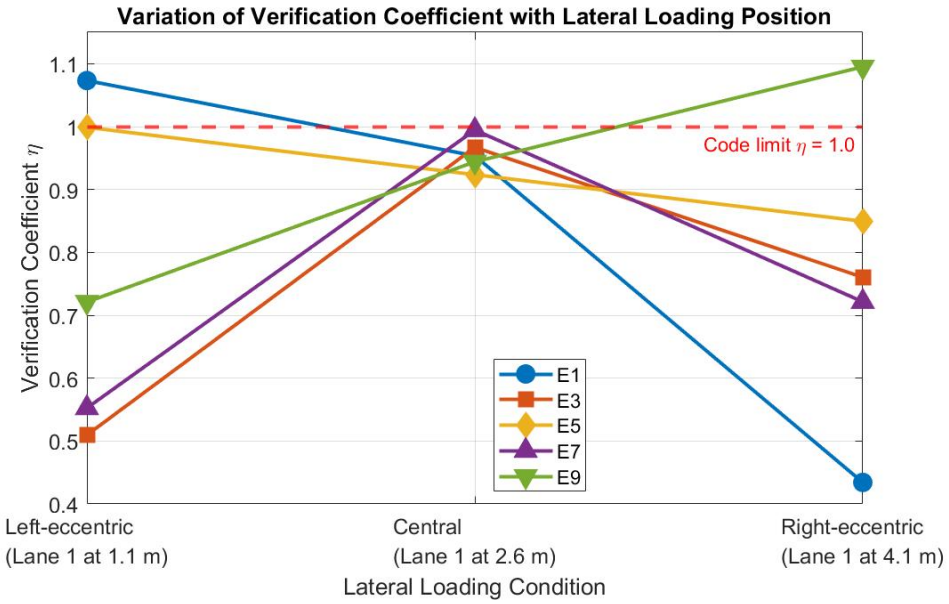


Fig. 8 Curves of verification coefficient at each slab versus lateral loading position

As shown in Table 3 and Fig. 8, the variation of η at each measurement point with lateral loading position is highly consistent with the lateral load-transfer characteristics of hollow slab bridges: E1, located on the left side of the deck, has its highest η value under left-eccentric loading (1.073), progressively decreasing to 0.434 as the load shifts to the right; E9, located on the right side of the deck, has its highest η value under right-eccentric loading (1.095), decreasing to 0.721 under left-eccentric loading; E7 has its highest η value under central loading (0.995), consistent with its position near the centerline of lane 2. For E3, η = 0.510 under left-eccentric loading, the low value resulting from the load shifting away from slab E3's position, which significantly reduces the longitudinal integration contribution, consistent with the pattern of lateral influence. The direction of variation of η at each point with lateral loading position corresponds one-to-one with its actual position on the deck, demonstrating good physical plausibility of the influence surface identification results in the lateral dimension.

E1 under left-eccentric loading (η = 1.073) and E9 under right-eccentric loading (η = 1.095) slightly exceed 1.0, reflecting that, after long-term service, the actual response of the edge slabs of the old hollow slab bridge under directly loaded conditions is slightly higher than the finite element theoretical prediction; the deviation magnitude is within 10%, which is within the normal range, with no abnormal sudden single-slab loading behavior indicative of hinge-joint failure observed.

It is worth noting that, if a hinge joint were to develop cracking damage, the η value of the directly loaded slab would become abnormally high under the eccentric loading condition, while the η value of the adjacent slab would become abnormally low, appearing in the figure as a sudden change in curve slope and anomalous crossing of adjacent measurement-point curves. In the results of this study, the slopes of all curves are smooth and the transitions between adjacent measurement points are natural, indicating that the hinge joints of each slab in the old carriageway of the Songjianghe River Bridge are transferring force normally, with good lateral coordinated working performance.

ISSN: 3007-9640 DOI: https://doi.org/10.70114/acmsr.2026.9.1.P127
Combined with dynamic comparison of influence surfaces identified at different time periods, the degradation trend of hinge-joint condition can also be tracked, enabling long-term health monitoring.

6. Conclusions

(1) A virtual load test method based on measured two-dimensional influence surfaces is proposed, combining the linear superposition principle with the Highway-Class I standard lane load. The method sequentially completes automatic determination of the most unfavorable load position, calculation of the virtual response, and solution of the verification coefficient, achieving rapid assessment of bridge load-carrying capacity without traffic closure; the calculation results can be directly compared with the code-specified verification-coefficient indices used in conventional static load testing.

(2) The verification coefficients η at each measurement point of the old simply supported hollow slab bridge of the Songjianghe River Bridge range from 0.924 to 0.995, all satisfying the code requirement of $\eta \leq 1.0$; the load-carrying capacity after strengthening meets the Highway-Class I standard. For the new five-span continuous box girder bridge, the η values at points B2 and B3 are 0.899 and 0.938, respectively, both clearly below 1.0, indicating ample load-carrying capacity reserve with overall stiffness exceeding the finite element theoretical prediction.

(3) Multi-lateral condition analysis based on the two-dimensional influence surface can effectively characterize the lateral load-transfer characteristics of hollow slab bridges. The variation of η at each measurement point with lateral loading position corresponds one-to-one with its actual position on the deck, with smooth curve slopes and natural transitions between adjacent measurement points; E1 under left-eccentric loading ($\eta = 1.073$) and E9 under right-eccentric loading ($\eta = 1.095$) slightly exceed 1.0, reflecting that the actual response of the edge slabs of the old bridge under directly loaded conditions is slightly higher than the theoretical model, with a deviation within 10% and no evidence of hinge-joint failure; the hinge joints of each slab in the old carriageway of the Songjianghe River Bridge exhibit good lateral coordinated working performance.

(4) The reliability of the proposed method depends on the accuracy of influence surface identification; the two-stage spatially weighted regularization method adopted achieves a mean deviation of 2.67% at the core measurement points, ensuring the engineering credibility of the verification-coefficient calculations. Combined with dynamic comparison of influence surfaces identified at different time periods, the degradation trend of structural performance can be tracked, extending the method from a single assessment to continuous health monitoring. Future research could further extend the proposed method to more complex bridge types such as cable-stayed and suspension bridges, and explore an online virtual load test framework incorporating real-time traffic flow data, to support intelligent maintenance decision-making for large bridge populations.

Acknowledgements

This work was supported by the Jilin Province Transportation Technology Enhancement and Application Project (2026-1-1).

References

[1] Ministry of Transport of the People's Republic of China. 2024 Statistical Bulletin on the Development of the Transportation Industry [R]. Beijing: Ministry of Transport, 2025.

[2] Ministry of Transport. Specification for Highway Bridge Load Testing: JTG/T J21-01-2015 [S]. Beijing: China Communications Press, 2015.

[3] Ko J M, Ni Y Q. Technology developments in structural health monitoring of large-scale bridges. Engineering Structures, 2005, 27(12): 1715-1725.

[4] Malekjafarian A, McGetrick P J, OBrien E J. A review of indirect bridge monitoring using passing vehicles. Shock and Vibration, 2015(1): 1-18.

ISSN: 3007-9640 DOI: https://doi.org/10.70114/acmsr.2026.9.1.P127
[5] Yang Y B, Lin C W, Yau J D. Extracting bridge frequencies from the dynamic response of a passing vehicle. Journal of Sound and Vibration, 2004, 272(3-5): 471-493.

[6] OBrien E J, Quilligan M J, Karoumi R. Calculating an influence line from direct measurements. Proceedings of the Institution of Civil Engineers-Bridge Engineering, 2006, 159(1): 31-34.

[7] Chen Z W, Yang W B, Li J, et al. Bridge influence line identification based on adaptive B-spline basis dictionary and sparse regularization. Structural Control and Health Monitoring, 2019, 26(6): e2355.

[8] Zheng X, Yang D H, Yi T H, et al. Bridge influence line identification from structural dynamic responses induced by a high-speed vehicle. Structural Control and Health Monitoring, 2020, 27(7): e2544.

[9] Zheng X, Yang D H, Yi T H, et al. Development of bridge influence line identification methods based on direct measurement data: A comprehensive review and comparison. Engineering Structures, 2019, 198: 109539.

[10] Hansen P C. Rank-Deficient and Discrete Ill-Posed Problems. Philadelphia: SIAM, 1998.

[11] Zheng X, Yang D H, Yi T H, et al. Bridge influence surface identification method considering the spatial effect of vehicle load. Structural Control and Health Monitoring, 2021, 28(8): e2769.

[12] Jian X, Xia Y, Chatzi E, et al. Bridge influence surface identification using a deep multilayer perceptron and computer vision techniques. Structural Health Monitoring, 2024, 23(3): 1765-1783.

[13] Ministry of Transport. General Specifications for Design of Highway Bridges and Culverts: JTG D60-2015 [S]. Beijing: China Communications Press, 2015.

[14] Tan G J, Gu J W, Wang W S, et al. A bridge influence line identification method and system based on two-stage spatially weighted regularization [P]. ZL 202610194457.3, 2026-03-17.

[15] Xia Q, Zhou Y C, Cheng Y Y, et al. Hinge joints performance assessment of a PC hollow slab bridge based on impact vibration testing. Structural Control and Health Monitoring, 2023, 1834669.